Shoemark, D., Sessions, R., Brancaccio, A., & Bigotti, M. G. (2018). Intraring allostery controls the function and assembly of a hetero-oligomeric class II chaperonin. *FASEB Journal*, *32*(4), 2223-2234. [fj.201701061R]. https://doi.org/10.1096/fj.201701061R

Intra-ring allostery controls the function and assembly of a hetero-oligomeric class II chaperonin

Deborah K. Shoemark[1], Richard B. Sessions[1], Andrea Brancaccio[1,2] and Maria Giulia Bigotti[1*]

[1]School of Biochemistry, University of Bristol, Bristol BS8 1TD, United Kingdom

[2]Istituto di Chimica del Riconoscimento Molecolare - CNR c/o Università Cattolica del Sacro Cuore, I-00168 Roma, Italy

[*]Corresponding author: University Walk, University of Bristol, Bristol BS8 1TD, United Kingdom. Email: g.bigotti@bristol.ac.uk, Tel. +44 (0)1173312138.

Short title: Allostery in the thermosome

NON STANDARD ABBREVIATIONS:

ATP: Adenosine triphosphate

CCT: Chaperonin containing TCP1

TriC: TCP1 ring complex

Cryo-EM: Cryo-electron microscopy

Ta: Thermoplasma acidophilum

PAGE: Polyacrylamide gel electrophoresis

BUDE: Bristol university docking engine

RhaD: Rhamnose dehydrogenase

AldT: Aldohexose dehydrogenase

WT: wild-type

ABSTRACT

Class II chaperonins are essential multi-subunit complexes that aid the folding of non-native proteins in the cytosol of archaea and eukarya. They use energy derived from ATP to drive a series of structural rearrangements that enable polypeptides to fold within their central cavity. These events are regulated by an elaborate allosteric mechanism in need of elucidation. We employed mutagenesis and experimental analysis, in concert with *in silico* molecular dynamics simulations and interface binding energy calculations, to investigate the class II chaperonin from *Thermoplasma acidophilum*. Here we describe the effects on the asymmetric allosteric mechanism and on hetero-oligomeric complex formation of a panel of mutants in the ATP binding pocket of the α and β subunits. Our observations reveal a potential model for a non-concerted folding mechanism optimized for protecting/refolding a range of non-native substrates under different environmental conditions, starting to unravel the role of subunit heterogeneity in this folding machine and establishing important links with the behaviour of the most complex eukaryotic chaperonins.

Key words: Molecular Chaperones, Protein Folding, Molecular Dynamics.

INTRODUCTION

Chaperonins are large (≈10^6 Da) oligomeric complexes aiding the folding of non-native polypeptides that are either newly synthesized or misfolded as a consequence of physiological or pathological cellular processes. They fulfil such a crucial role in all living organisms by sequestering, through a series of ATP-driven and highly controlled allosteric conformational rearrangements, non-native polypeptides in a central cavity where they can fold unperturbed by the cellular environment (1, 2). Chaperonins are composed of two multi-subunit rings stacked back-to-back to form a toroidal cylinder enclosing an internal space, often referred to as the folding chamber. This architecture is common to chaperonins from eubacteria and cell organelles (class I) and those from archaea and the eukaryotic cytosol (class II). The latter group is structurally more complex than its bacterial counterpart, mostly owing to heterogeneity in subunit composition. The type of subunits forming each 8 (occasionally 9) (3) membered ring ranges from the 1-3 found in archaebacterial chaperonins, or thermosomes, to the 8 different subunits of eukaryotic chaperonin CCT/TriC (for chaperonin containing TCP-1/TCP-1 ring complex). Despite some degree of sequence variability, the high-resolution crystal and cryo-EM structures of the archaeal (4-6) and eukaryotic (7-9) class II chaperonins reveal that all subunits share an identical domain organization. This consists of an equatorial domain that forms the inter-ring interface and contains the ATP-binding site, an apical domain responsible for the interaction with non-native substrates and containing most of the intra-ring contacts between subunits, and an intermediate domain, connecting the other two, which acts as a hinge that is fundamental for the propagation of allosteric signals. Furthemore, a helical module at the tip of the apical domain acts as a lid closing the folding chamber upon ATP hydrolysis.

Despite considerable advances made in recent years, many of the structural and functional details behind type II chaperonins activity and their relation to the allosteric behaviour of these ATP-ase machines are still poorly understood. This is mainly due to the intrinsic structural complexity of class II chaperonins, whose hetero-oligomeric nature makes a recombinant approach particularly challenging As a matter of fact, only very recently Yamamoto and colleagues succeeded in producing sufficiently large amounts of CCT from a thermophilic fungus in *E. coli* for recombinant analysis (10). Indeed, most of the information available to date comes from *in vitro* studies conducted on CCT purified from mammalian and yeast cells. In a pioneering study, ATP binding/hydrolysis site-directed mutants of different subunits of CCT from *Saccharomyces cerevisiae* highlighted a hierarchy in ATP binding/hydrolysis amongst subunits possibly independent of their intrinsic structural role in the oligomer (11, 12). Such a complex scenario has been corroborated by a series of mutagenesis studies on *S. cerevisiae* CCT (13-15) showing a gradient of ATP affinities in the different

subunits, according to which they group together on two opposite sides of each ring. This has been confirmed by cryo-EM analysis of a newly identified state, partially preloaded with nucleotide, and of the ATP-bound state (16). Further analysis of the data on ATP-site mutants led to the proposal of a model describing an intra-ring sequential allosteric mechanism of ATP hydrolysis by CCT (17). It has been speculated that such a complex mechanism, based on the differential characteristics and behaviour of the subunits, could increase the efficiency of folding of multidomain proteins by allowing their release from the chaperonin domain by domain in a sequential order (15, 17-19).

Thermosomes are well-placed to provide further insights into this phenomenon, as their reduced subunit heterogeneity correlates well with the lower abundance of multidomain proteins in the archaeal proteome compared with their eukaryotic counterparts (20, 21).

Despite their lower complexity in subunit composition, hetero-oligomeric thermosomes present similarities with the allosteric behaviour of CCT (22-24). Indeed, it has been shown that the thermosome from the acidophilic archaeon *Thermoplasma acidophilum* (*Ta* thermosome), a hexadecamer composed of α and β subunits, has a biphasic ATP-ase activity, indicative of the presence of two different classes of ATP binding sites (22, 25).

The *Ta* thermosome has been taken as a model for class II chaperonins studies (22, 25-28) since it was the first of such proteins whose structure was solved at high resolution by X-ray crystallography (4). It is composed of two octameric rings of alternating α and β subunits. Our recombinant system for the *Ta* thermosome employs an intra-loop His_6-tag in each α-subunit and allows for a carefully balanced over-expression of α and β subunits in *E. coli*. This system produces unprecedented amounts of functional αβ-thermosome hexadecamers (29) and has served well for the efficient expression and purification of mutants for this study. A panel of single residue mutants was chosen aimed at impairing either ATP binding or hydrolysis in the α and β subunits individually. Experiments were devised to explore whether each mutant a) altered ATP binding/hydrolysis in the system, b) influenced subunit heterogeneity in thermosome assembly c) affected the refolding behaviour and d) allowed us to begin to pinpoint the specific contribution of each subunit to the folding cycle. Furthermore, given that some of the single point-mutations in the ATP binding pocket may also affect the hetero-oligomeric state of the whole complex, molecular dynamics simulations were employed to investigate the propensity towards the native $\alpha_8\beta_8$ oligomeric state and its molecular determinants.

MATERIALS AND METHODS

Site-directed mutagenesis and preparation of mutants

A construct for the over-expression in *E.coli* of a 8x(His_6)-tagged α_8/β_8 *Ta* thermosome (aK144HTTherm) (29) was used as template for site-directed mutagenesis. All mutants were obtained using the Quikchange Lightning Site-Directed Mutagenesis kit (Agilent Technologies) according to the manufacturer instructions, and checked by automated sequencing. The variant constructs were used to transform *E. coli* BL21(DE3) Codon Plus-RIL cells, and the mutants expressed and purified to homogeneity as described elsewhere for the wild-type thermosome (29). The integrity of the complexes was checked by high-resolution size-exclusion chromatography on a Superose 6 Increase column (GE Healthcare) and by native-PAGE (3-12% acrylamide), and the composition in subunits was determined by Tris-Acetate SDS-PAGE (7% acrylamide) of the purified proteins. A Superose 6 column was used as a further purification step in order to isolate the hexadecameric species from smaller oligomers and isolated single subunits. All the enzymes used for nucleic acid manipulation were either from New England Biolabs or Roche, and the kits used for DNA prepping and extraction/purification were from Qiagen.

Sequence alignment

The chaperonins sequences were aligned in MUSCLE 3.8 (30) via the resources of EMBL/EBI (http://www.ebi.ac.uk/Tools/msa), and are presented in BoxShade 3.21 (http://www.ch.embnet.org/software/BOX_form.html). The following NCBI coders refer to the aligned sequences from different species: *Thermoplasma acidophilum*, alpha: CAC12109; and beta: WP_010901684; *Escherichia coli*, GroEL: WP_004201176; *Methanococcus maripaludis*, alpha: WP_011171459; *Sulfolobus solfataricus*, alpha: WP_009992283; beta: 4XCG_B and gamma: AAK43104; *Saccharomyces cerevisiae*, alpha: NP_010498; beta: NP_012124; gamma: NP_012520; delta: NP_010138; epsilon: NP_012598; zeta: NP_010474; eta: NP_012424 and theta: NP_012526.

Modelling and Molecular Dynamics Simulations

Molecular graphics manipulations and visualisations were performed using VMD-1.9.1 and Chimera-1.10.2 (31). Chimera was used to overlay subunits from the 1A6D crystal structure to generate the $alpha_{16}$ and $beta_{16}$ assemblies. The GROMACS-4.6.7 suite of software was used to set up, energy minimise and perform the molecular dynamics simulations

Scwrl4 (32) was used to pack the side chains. Pdb2gmx was used to prepare the assemblies using the v-site hydrogen option to allow a 5 femtoseconds time step. Hydrogen atoms were added consistent with pH 7 and parameterised with the AMBER-99SB-ildn forcefield. Each complex was surrounded by a box 2 nm larger than the polypeptide in each dimension, and filled with TIP3P water. Random water molecules were replaced by sodium and chloride ions to give a neutral (uncharged overall) box and an ionic strength of 0.15 M. Each box contained ~ 880,000 atoms. Each assembly was subjected to 5000 steps of energy minimisation prior to position restrained and subsequent molecular dynamics simulations.

MD simulations were run for each of the wild-type assemblies for 50 ns in order to equilibrate the systems and data were then acquired for a further 50 ns. The ATP binding and hydrolysis mutations were produced in Chimera from these equilibrated assemblies, energy minimised, position restrained, and simulated for 50 ns.

Simulation details: all simulations were performed as NPT ensembles at 298 K using periodic boundary conditions. Short range electrostatic and van der Waals' interactions were truncated at 1.4 nm, while long range electrostatics were treated with the particle-mesh Ewald's method and a long-range dispersion correction applied. Pressure was controlled by the Berendsen barostat and temperature by the V-rescale thermostat. The simulations were integrated with a leap-frog algorithm over a 5 fs time step, constraining bond vibrations with the P-LINCS method. Structures were saved every 0.1 ns for analysis and each run over 50 ns. Simulation data were accumulated on the UK supercomputer Archer.

In each case the analysed trajectories from the last 50 ns run were written out as pdb "snapshots". Each subunit was then extracted from the pdb (maintaining the same coordinates) and the binding energy of the interfaces calculated using BUDE (Bristol University Docking Engine) (33). Microsoft excel was used to graphically display the results. Images were produced with chimera and Microsoft Paintshop or GIMP (GNU Image Manipulation Program [https://www.gimp.org/]).

Steady-state ATPase measurements

ATP hydrolysis was measured using a modification of the classic Malachite green reagent (34) (Biomol Green, Enzo Life Sciences) allowing for thermostable and reliable measurements of inorganic phosphate release at 55°C. The standard reaction buffer used in all experiments was 25 mM Tris-HCl (pH 7.5), 50mM KCl, 20mM $MgCl_2$ and 50mM NaCl. The reactions were started by adding the thermosome to a temperature-equilibrated reaction mixture containing the reaction buffer and ATP at increasing concentrations, in a final volume of 100 μl; all the data were collected, for a minimum of 7 minutes, also in the absence of thermosome in order to

correct for ATP spontaneous hydrolysis at 55°C. Data for all the mutants were averaged over a minimum of three independent experiments, and were fitted to a standard one site Michaelis-Menten equation, assuming only one type of subunit is active at a time.

Substrate refolding assays

The refolding yield of the recombinant substrates *Ta* Ramnose Dehydrogenase (RhaD) and *Ta* Aldohexose Dehidrogenase (AldT) was assessed as described elsewhere (29). The lag phase of the recovery in activity, not reported in the graphs for clarity, was typically of 2-3 minutes and was not significantly affected in any of the variants analysed, either in the absence or presence of ATP.

RESULTS

Point-mutations in the ATP-binding pocket influence oligomerization

All the mutagenesis work was performed on a construct for the genetic manipulation and over-expression of the *Ta* thermosome previously described (29). Fig. 1A shows a cartoon representation of the 8x(His_6)-tagged hetero-oligomer thus produced. All the mutants described, either in α_8/β_8 or α_{16} form (see Table 1 for reference), were purified to homogeneity following the purification protocol described for the wild-type protein (29) and their integrity checked by high resolution size exclusion chromatography and native PAGE (Fig. 2B and 2C). The final yield varied between 5 and 10 mg/litre of bacterial culture; like the WT, all mutants, with the exception of T96Vβ and T97Vα, are remarkably stable in solution and can be stored at 4°C for days at a time.

Based on the nucleotide-bound structure determined at high resolution by X-ray crystallography (4) and/or on analogies with functional mutants in GroEL (35) and yeast CCT (14), two kinds of mutations were inserted in either of the subunits in turn, i.e. those abolishing ATP hydrolysis and those abolishing ATP binding altogether (Fig. 1A and 1B). In the former case an aspartate residue, universally conserved in the active site of all chaperonins and shown to be involved in ATP hydrolysis both in GroEL and CCT (Fig. 1C), was mutated in the α and β subunits one at a time. Residues Asp93β and Asp94α (the greek symbols identify the subunit targeted) were initially mutated to lysines, with different outcomes for the two subunits. The mutant D93Kβ expressed with a yield comparable to that of the wild-type and assembled correctly into an $\alpha_8\beta_8$ hetero-oligomer. D94Kα failed to do this, and the only complex that could be purified was a homo-oligomer composed of α subunits (α_{16}) (Fig. 2A and 2B). The same result was obtained when mutating Asp94α to a glutamate residue (with a

lower yield of intact α_{16} complex): finally, a correctly assembled $\alpha_8\beta_8$ thermosome was produced with the substitution Asp94α to alanine (Fig. 2A and 2B).

Similarly, a complex and unexpected pattern emerged when mutating residues Thr96β and Thr97α, that are part of the highly conserved P loop, as first discussed by Reissmann et al. (15) (Fig.1C). These mutations were designed to interfere with ATP binding by abolishing the stabilising hydrogen bonds that those residues establish with the γ-phosphate of the ATP molecule in the nucleotide pocket of the β and α subunits, respectively (4) (Fig. 1A-C). The conservative mutation of these threonines to valines in either of the subunits, prevented them from assembling into $\alpha_8\beta_8$ hetero-oligomers, and again only α_{16} complexes could be isolated, albeit with reduced yield and stability compared to the WT (as deduced from an increased susceptibility to proteolytic degradation during purification, data not shown). As a result, Thr157α and Thr158β were chosen as less conserved (Fig.1C) and possibly less disruptive alternatives for impairing ATP binding, based on their involvement in a hydrogen bond with the nucleoside ribose in the ATP binding pocket of the respective subunits. These mutants (T157Aα and T158Aβ) successfully formed $\alpha_8\beta_8$ complexes (Fig. 2A and 2B).

Calculation of subunit interface energies successfully predicts the *in vivo* oligomeric state

In order to investigate the determinants of the hetero-oligomeric state of the *Ta* thermosome, the first essential step was to analyse the intrinsic propensity of the wild-type subunits to assemble into a hetero-oligomeric complex. Experiments *in vitro* showed that when both subunits were co-expressed in *E. coli*, the $\alpha_8\beta_8$ assembly formed readily. However, if the β subunits were absent or limiting, the α_{16} thermosome was formed. This is in stark contrast to the β_{16} assembly which has not been observed experimentally either in the presence or absence of the α subunit. One of the possible ways to approach such complex phenomena is to use *in silico* analysis, through molecular dynamics simulation of the assemblies combined with assessment of the inter subunits energies using the BUDE (Bristol University Docking Engine) (33) empirical free energy forcefield. Chaperonins are large systems, typically comprised of 870,000 atoms (including explicit water), so the simulations were carried out on the UK supercomputer Archer as described in Materials and Methods. The wild-type assemblies of the $\alpha_8\beta_8$, α_{16} and the β_{16} were simulated for 50 ns to allow the systems to equilibrate. Subsequently each system was simulated for a further 50 ns and structures extracted at regular intervals for interface energy analysis. From these “snapshots”, each subunit of each of the assemblies was analysed for its global interface energy with respect to the rest of the thermosome (see Fig. 3A and 3B) using BUDE (36, 37). Fig. 3C shows the global inter-subunit energies, again averaged over each 50 ns trajectory, and figure 3D reports the inter-subunit averaged global interface energies profile over time. The results of this analysis nicely

correlate with *in vitro* experimental observations, predicting that formation of the $\alpha_8\beta_8$ and α_{16} assemblies is favoured over that of the β_{16}.

Further calculations were performed between neighbouring pairs of subunits to explore the contributions of the intra-ring and inter-ring interface energies to subunit assembly as indicated in Fig. 3A and B and Table 2. These data revealed that the intra-ring energy contribution is comparable for $\alpha_8\beta_8$ (-450 kJ/mol) and the α_{16} (-447 kJ/mol) assemblies but is less favourable for the β_{16} assembly (-401 kJ/mol). In contrast, the inter-ring energy for β_{16} is somewhat better than for $\alpha_8\beta_8$ (-123 kJ/mol and -114 kJ/mol, respectively), but insufficient to outweigh the less favourable β_{16} intra-ring energy. Moreover, the diagonal interactions, i.e. those of subunit 2 with subunits 4 and 6 in Fig. 3B (see last column in Table 2), are weak in comparison to those with the closer neighbours i.e. subunits 1, 3 and 5.

The ATP binding and hydrolysis mutants characterised in this study revealed interesting changes to the assembly propensity of thermosome molecules *in vitro* (see Table 1). The same approach was used to explore how these mutations influence subunit interface energies. Unfortunately, the signal to noise in these experiments concealed any effect other than the consistently reduced interface energies observed for the β_{16} complexes (Fig. S1). We suggest that the amount of sampling required by molecular dynamics to attain an appropriate signal to noise for the energy profiles is beyond current resources.

Differential behaviour of the α and β subunits towards ATP

The variants where ATP-hydrolysis was impaired by mutation of the catalytically essential D93β or D94α residues were first analysed by steady-state ATP-ase kinetics. Indeed, previous studies established that the WT *Ta* thermosome, both in its native (27) and recombinant forms (22, 29) shows a biphasic ATPase profile indicating the presence of two classes of ATP binding sites, either reflecting negative cooperativity between rings, whereby only one ring is active at low ATP concentration, or a differential behaviour of the α and β subunits, or both. A thermally stable colorimetric essay (34) was used to record the steady-state production of inorganic phosphate upon ATP hydrolysis at 55°C in the presence of thermosome as a function of ATP concentration, and the results are plotted in Fig. 4A and 4B. A linear dependence of the maximum hydrolytic rates on protein concentration was measured for all variants (Fig. 4B, inset), which allowed us to rule out the possibility of an equilibrium between heterogeneous oligomeric states with different ATP-ase activities. Crucially, these and all the ATP-ase activity experiments were performed on the hexadecameric complexes isolated by size-exclusion chromatography on a semi-preparative Superose 6 column to ensure homogeneity.and to exclude the presence of mixed populations of smaller oligomers/single subunits that elute

at longer retention times (see Fig. 2C). All data were fitted to a single-site Michaelis-Menten equation, and the results are reported in Table 1. By contrast with what observed for the WT, the two single mutants analysed here only show one phase to the saturation (Fig. 4A), indicative of a single class of binding sites. Furthermore, the α-only thermosome (WTα_{16}) complex (obtained when the α subunit is expressed in *E. coli* in the absence of the β) also shows a non-cooperative single-transition ATPase profile (Fig. 4B) and the hydrolysis mutant D94Kα, which assembles only as D94Kα_{16}, displays no measurable ATPase activity at all. D93Kβ ($\alpha_8\beta_8$), where ATP hydrolysis can only occur on the WTα subunits, displays a saturation midpoint comparable to that of the WT weak sites. Conversely, the apparent K_M for mutant D94Aα ($\alpha_8\beta_8$), in which ATP hydrolysis must be assigned to the WTβ subunits, corresponds more closely (although ~5-fold weaker) to the K_M calculated for the WT tight sites.

These results are mirrored by differential ATP turnover values, with the α subunits displaying a hydrolytic rate almost two times lower than that of the β subunits, again in line with what observed for the two transitions of the WT complex. Notably, when assembling into a α-only complex such as WTα_{16}, the α subunits display a diminished rate of turnover despite a slightly higher affinity for ATP (Fig 4B).

Somewhat surprisingly, none of the ATP-binding mutants, in either subunit, shows any detectable ATPase activity.

Differential behaviour of the α and β subunits towards non-native substrates

The ability of the ATP hydrolysis mutants to aid folding of a thermophilic protein substrate was explored. Fig. 4C reports the refolding yield of the unfolded endogenous substrate rhamnose dehydrogenase from *T. acidophilum* (*Ta* RhaD, shown to be an easily assayable substrate in such refolding experiments) (29) measured as recovery in enzymatic activity upon refolding in the presence of the mutant chaperonins. Specifically, the renaturation assay was initiated by extensive dilution of chemically denatured (in 8 M urea) *Ta* RhaD into a buffer containing an excess of either D93Kβ, D94Kα or D94Aα, with or without ATP added. RhaD catalyses the $NADP^+$ dependent oxidation of L-rhamnose, so the recovery in activity at 55 °C was monitored spectrophotometrically by the rate of increase in absorbance at 340 nm that follows the reduction of $NADP^+$ to NADPH, as compared with the activity of the native enzyme. The percentage of recovery calculated for all mutants is reported in Table 1. In the present work substrate denaturation was induced with urea instead of the previously used GdnHCl (29). Urea was used here as a chaotropic agent in order to avoid any effects that the ionic strength of GdnHCl could exert (38, 39). The wild-type thermosome shows a remarkable refolding activity even in the absence of ATP, with a yield of folded RhaD of about 68% that increases to values close to

100% when ATP is added to the refolding mixture. All mutants (except T97Vα) are still capable, although less than the WT, of aiding the renaturation of unfolded RhaD. The most efficient of the $\alpha_8\beta_8$ mutant complexes is D93Kβ, and the data indicate that, when only the α subunit is active in hydrolysing ATP, the thermosome ability to fold substrates is slightly less than half that of the WT; when ATP hydrolysis occurs only on the β subunit, as in D94Aα, the folding activity is further diminished. The inset in Fig. 4C shows the recovery in activity of unfolded RhaD in the presence of the α-only variants WTα_{16} and D94Kα α_{16}. Both complexes retain a certain, albeit diminished, degree of refolding ability compared to WT $\alpha_8\beta_8$, demonstrating that the β subunit is not indispensable for the *Ta* thermosome to fulfil its function.

The results of refolding assays on the ATP binding mutants are plotted in Fig. 4D. Despite their similar behaviour towards ATP, the two complexes promote renaturation to different extents, with T158Aβ displaying a refolding activity which is double that of T157Aα.

DISCUSSION

We have here identified a series of residues that individually influence the oligomerisation state of the *Ta* thermosome, highlighting how the composition of the ATP-binding pocket is also crucial for the correct assembly of the entire chaperonin complex. Indeed, the mutations altering assembly map into one of the regions with the highest degree of sequence conservation in all chaperonins (as reported in Fig. 1C), a module within the ATP-binding pocket defined as P-loop (15), confirming its importance both from a structural and functional point of view. Specifically, mutations in both subunits of the Asp and last Thr residue of the GDGTT motif representing the P-loop have a major effect on the formation of $\alpha_4\beta_4$ rings. To investigate the energetic contribution of these residues to the correct assembly of the oligomer we used computational methods High performance computing (Archer – UK supercomputer and Bluegem BrisSynBio) and use of v-sites in GROMACS has made exploring these large systems by all-atom molecular dynamics simulations more accessible. Moreover, advances in docking software such as BUDE have allowed the contribution of interface energies for individual subunits to be calculated. Although the contributions of individual P-loop residues to the assembly propensity proved too subtle to be picked up by this technique (Fig.S1 and S2), their application to a system as complex as the thermosome was successful in predicting the preference of its WT subunits for assembly into either an $\alpha_8\beta_8$ or an α_{16} oligomer with respect to the β_{16} form (Fig 3A). The latter is energetically disfavoured and to our knowledge has never been isolated *in vivo* (22, 29). This result gives computational support to the empirical observation that, when expressed and purified separately and then mixed, the α and β subunits fail to reconstitute $\alpha_8\beta_8$ complexes. The assembly of αβ is favoured, as shown by the exclusive

isolation of hetero-hexadecamers when the two subunits are co-expressed in equal amounts (22) and as also recently reported for TF55, the chaperonin from *Sulfolobus solfataricus* (40).

Interestingly, the interaction energies between two β_8 rings were predicted to be more favourable to the hexadecamer formation than the interaction energy between two $\alpha_4\beta_4$ rings, but this appears to be insufficient to overcome the energetic cost of assembling an all-β ring. These results reflect the necessity for each ring to incorporate α subunits in order to have folding activity. Incorporation of the beta subunits, with their predicted stronger inter-ring interactions and weaker intra-ring interactions may provide an appropriate degree of flexibility essential for an efficient folding cycle. It should be noted that the strict subunit composition ($\alpha_8\beta_8$) found in the thermosome from the *Ta* organism (4) is not a characteristic of all hetero-oligomeric archaeal chaperonins. In cases where three subunits are present, assemblies can form from a variety of subunit combinations, such that they can be individually dispensable for cell viability (40, 41). Such redundancy in subunits has been proposed to be a means to adapt to different environmental conditions via a range of subunit arrangements.

We observed that the *Ta* WTα_{16} recombinant complex has a reduced ATP-ase activity not only with respect to WT $\alpha_8\beta_8$ but also to the D93Kβ mutant (Fig.4A and 4B), where only the α subunits are active. Moreover, the refolding yield of WTα_{16} is not only half of that of the wild-type $\alpha_8\beta_8$ complex, but also comparable to that of D93Kβ both in the absence and presence of ATP (Fig. 4C). These results suggest that the presence of the β subunits (even when inactive) does enhance the overall hydrolysis process as well as the intrinsic folding capacity of the complex, ultimately confirming that the alternation of different subunits within a ring has a key role in the folding cycle.

The mutational analysis reported here confirms that the biphasic allosteric behaviour observed in the wild-type *Ta* thermosome arises from the presence of two different chains that display individual characteristics with respect to ATP binding and hydrolysis, as well as to the unfolded substrate. Although the possible contribution of the double-ring structure to asymmetry needs to be investigated, our results allow us to propose a tentative model for the interplay of events taking place in a *Ta* thermosome ring upon ATP binding and hydrolysis (Fig. 5). The first evidence to consider is that when ATP binding is blocked in either of the subunit types, the complex is unable to hydrolyse ATP, implying that adjacent subunits both need to be nucleotide-binding competent for ATP-cycling to proceed at steady state. Fig. 5A shows the possible scenario of complete block of the cycle when the two ATP-binding mutants (T157Aα and T158Aβ) are challenged with ATP, assuming that the unmodified subunits in each case are still able to bind ATP. The scheme takes into account that the blocking

of ATP binding to one subunit could impair ATP cycling in the adjacent subunit either at the stage of ATP hydrolysis (complex one) or at that of ADP+Pi release (complex 2, boxed).

Secondly, mutants where ATP-hydrolysis is impaired in either of the subunits (D94Aα and D93Kβ) still undergo ATP-cycling in the remaining wild-type subunits. Interestingly, based on the complete lack of hydrolysis activity shown by the mutant α_{16} complex D94Kα, it was possible to establish that in the *Ta* thermosome modification of Asp93/94 effectively abolishes ATP hydrolysis in the subunit carrying it (unlike the equivalent case for GroEL, in which hydrolysis is only partially affected) (35).

Thirdly, the kinetic constants reported in Table 1 show how the β subunit is more ATP-ase active (displaying a lower K_M and a higher k_{cat}) than the α subunit, thus confirming that the asymmetry observed in the *Ta* thermosome cycle (22, 29) depends, at least partly, on the different contributions of ATP-ase activity offered by the two subunits. This behaviour establishes a link with the eukaryotic chaperonin CCT, whose subunits have been classified as "weak" or "strong" depending on their response to ATP (with only 4 subunits per ring at a time binding ATP in physiological conditions) (15, 42).

It was previously reported that ATP-hydrolysis in the *Ta* thermosome occurs rapidly after binding and that the rate-limiting step of the ATP-ase cycle is product release of either ADP, phosphate, or both. In other words, the hydrolysis product-bound species is the most populated at steady state (25). Based on all the evidence taken together, it is possible to envisage a cycle in which ATP must be bound to one subunit for hydrolysis products to be released from the adjacent one. This scenario for the two hydrolysis mutants is shown in Fig. 5B, where a model for a cycle carried out by the ATP-ase competent subunit is proposed with the adjacent, ATP-ase deficient subunit permanently loaded with ATP. For graphical clarity, the scheme only reports the cycle of events in which ATP binds to the β subunit (i.e. the most ATP-ase active) first; although not included in the panel, a similarly asymmetric cycle comprising a complex in which the α subunit binds ATP first is also possible.

How do the observed refolding activities fit into these models? It has to be noted that the *Ta* thermosome facilitates protein folding *in vitro* to some degree even in the absence of ATP, as do all the mutants, except the highly destabilised T97Vα. We ascribe this to its intrinsic ability to bind unfolded substrates and prevent the aggregation phenomena they would naturally undergo. It has been shown in other thermosomes that the substrate binding sites of the apical domains, which are exposed in the apo-form, are still accessible after the structural rearrangements driven by ATP binding, but not after hydrolysis (43). When they are impaired in ATP

binding or hydrolysis, the α or β subunits of the *Ta* thermosome are stalled in the cycle either in the apo- or in the ATP-bound states respectively, maintaining substrate-binding competency.

Interestingly, ATP-binding and/or hydrolysis impairment has a larger effect on folding capacity when the weak (α) subunits are targeted: although in need of further investigation, these findings could indicate an intrinsically higher affinity of the α subunits for unfolded substrates. The same phenomenon, but of opposite sign, has been observed on CCT from *S. cerevisiae*, where ATP-hydrolysis mutants of the strong (β-equivalent) subunits were found to affect cell viability the most (14, 15). This was interpreted as a way to connect, through subunit-substrate (or substrate domain) specificity, the ATP-cycling trajectory to a specific folding pathway (17).

The asymmetry in the ATP-ase cycle described here points to a folding mechanism of the thermosome from *T. acidophilum* with distinct characteristics relative to that of the homo-oligomeric archaeal chaperonins, whose structural analysis by cryo-EM (6, 43, 44) and X-ray crystallography (5, 45) has been pivotal for elucidating many molecular details of the ATP dependent behaviour of class II chaperonins. Moreover, our results exclude the possibility of a concerted response to ATP as observed in GroEL, and draw important similarities between the allosteric mechanisms of hetero-oligomeric thermosomes and eukaryotic class II chaperonins. Based on the evidence to date, a tentative model for the ATP-ase cycle of the WT complex is proposed in Fig.5C. Allosteric communication between alternating subunits with specific behaviours towards ATP, by maintaining "next neighbour" asymmetry, allows the non-native substrate the opportunity to remain in contact with the chaperonin, either by interacting with the apo or ATP-bound subunits, or by having sufficient time to fold within the chamber. It may be that such asymmetric behaviour could provide a way for the *Ta* thermosome to enhance and modulate its sensitivity to variations in ATP levels under different cellular conditions; this 'tunable' behaviour towards ATP might be an intrinsic property of class II chaperonins, as recently proposed by Lopez and colleagues (46). Subunits asymmetry could also reduce the need for full or synchronised lid closure, allowing the accommodation of a greater range of substrate sizes. This hypothesis is supported by the structural work of Clare and colleagues (47), who have demonstrated that the partially closed ATP-bound state, with its relatively large chamber, can accommodate substrates which would otherwise be excluded from the smaller lumen of the fully closed state.

ACKNOWLEDGEMENTS

This work was supported by a Wellcome Trust Career Re-entry Fellowship to M.G.B. The authors would like to thank the Advanced Computing Research Centre at Bristol University (Bluecrystal) for access to computational resources and HECBiosim for allocating time on the UK's supercomputer Archer.

AUTHOR CONTRIBUTIONS

M.G.B. and A.B. conceived the project and the experimental work. M.G.B. carried out and analysed all the experiments. D.K.S. and R.B.S. conceived and performed the *in silico* analyses. M.G.B., D.K.S. and A.B. wrote the manuscript.

REFERENCES

1. Lopez, T., Dalton, K., and Frydman, J. (2015) The Mechanism and Function of Group II Chaperonins. *J Mol Biol* **427**, 2919-2930
2. Skjaerven, L., Cuellar, J., Martinez, A., and Valpuesta, J. M. (2015) Dynamics, flexibility, and allostery in molecular chaperonins. *FEBS letters* **589**, 2522-2532
3. Conway de Macario, E., Robb, F. T., and Macario, A. J. (2016) Prokaryotic Chaperonins as Experimental Models for Elucidating Structure-Function Abnormalities of Human Pathogenic Mutant Counterparts. *Frontiers in molecular biosciences* **3**, 84
4. Ditzel, L., Lowe, J., Stock, D., Stetter, K. O., Huber, H., Huber, R., and Steinbacher, S. (1998) Crystal structure of the thermosome, the archaeal chaperonin and homolog of CCT. *Cell* **93**, 125-138
5. Huo, Y., Hu, Z., Zhang, K., Wang, L., Zhai, Y., Zhou, Q., Lander, G., Zhu, J., He, Y., Pang, X., Xu, W., Bartlam, M., Dong, Z., and Sun, F. (2010) Crystal structure of group II chaperonin in the open state. *Structure* **18**, 1270-1279
6. Zhang, J., Ma, B., DiMaio, F., Douglas, N. R., Joachimiak, L. A., Baker, D., Frydman, J., Levitt, M., and Chiu, W. (2011) Cryo-EM structure of a group II chaperonin in the prehydrolysis ATP-bound state leading to lid closure. *Structure* **19**, 633-639
7. Cong, Y., Baker, M. L., Jakana, J., Woolford, D., Miller, E. J., Reissmann, S., Kumar, R. N., Redding-Johanson, A. M., Batth, T. S., Mukhopadhyay, A., Ludtke, S. J., Frydman, J., and Chiu, W. (2010) 4.0-A resolution cryo-EM structure of the mammalian chaperonin TRiC/CCT reveals its unique subunit arrangement. *Proc Natl Acad Sci U S A* **107**, 4967-4972
8. Dekker, C., Roe, S. M., McCormack, E. A., Beuron, F., Pearl, L. H., and Willison, K. R. (2011) The crystal structure of yeast CCT reveals intrinsic asymmetry of eukaryotic cytosolic chaperonins. *EMBO J* **30**, 3078-3090

9. Kalisman, N., Schroder, G. F., and Levitt, M. (2013) The crystal structures of the eukaryotic chaperonin CCT reveal its functional partitioning. *Structure* **21**, 540-549
10. Yamamoto, Y. Y., Uno, Y., Sha, E., Ikegami, K., Ishii, N., Dohmae, N., Sekiguchi, H., Sasaki, Y. C., and Yohda, M. (2017) Asymmetry in the function and dynamics of the cytosolic group II chaperonin CCT/TRiC. *PLoS One* **12**, e0176054
11. Lin, P., Cardillo, T. S., Richard, L. M., Segel, G. B., and Sherman, F. (1997) Analysis of mutationally altered forms of the Cct6 subunit of the chaperonin from Saccharomyces cerevisiae. *Genetics* **147**, 1609-1633
12. Lin, P., and Sherman, F. (1997) The unique hetero-oligomeric nature of the subunits in the catalytic cooperativity of the yeast Cct chaperonin complex. *Proc Natl Acad Sci U S A* **94**, 10780-10785
13. Shimon, L., Hynes, G. M., McCormack, E. A., Willison, K. R., and Horovitz, A. (2008) ATP-induced allostery in the eukaryotic chaperonin CCT is abolished by the mutation G345D in CCT4 that renders yeast temperature-sensitive for growth. *J Mol Biol* **377**, 469-477
14. Amit, M., Weisberg, S. J., Nadler-Holly, M., McCormack, E. A., Feldmesser, E., Kaganovich, D., Willison, K. R., and Horovitz, A. (2010) Equivalent mutations in the eight subunits of the chaperonin CCT produce dramatically different cellular and gene expression phenotypes. *J Mol Biol* **401**, 532-543
15. Reissmann, S., Joachimiak, L. A., Chen, B., Meyer, A. S., Nguyen, A., and Frydman, J. (2012) A gradient of ATP affinities generates an asymmetric power stroke driving the chaperonin TRIC/CCT folding cycle. *Cell Rep* **2**, 866-877
16. Zang, Y., Jin, M., Wang, H., Cui, Z., Kong, L., Liu, C., and Cong, Y. (2016) Staggered ATP binding mechanism of eukaryotic chaperonin TRiC (CCT) revealed through high-resolution cryo-EM. *Nat Struct Mol Biol* **23**, 1083-1091
17. Gruber, R., Levitt, M., and Horovitz, A. (2017) Sequential allosteric mechanism of ATP hydrolysis by the CCT/TRiC chaperone is revealed through Arrhenius analysis. *Proc Natl Acad Sci U S A* **114**, 5189-5194
18. Rivenzon-Segal, D., Wolf, S. G., Shimon, L., Willison, K. R., and Horovitz, A. (2005) Sequential ATP-induced allosteric transitions of the cytoplasmic chaperonin containing TCP-1 revealed by EM analysis. *Nat Struct Mol Biol* **12**, 233-237
19. Joachimiak, L. A., Walzthoeni, T., Liu, C. W., Aebersold, R., and Frydman, J. (2014) The structural basis of substrate recognition by the eukaryotic chaperonin TRiC/CCT. *Cell* **159**, 1042-1055

20. Vogel, C., Bashton, M., Kerrison, N. D., Chothia, C., and Teichmann, S. A. (2004) Structure, function and evolution of multidomain proteins. *Curr Opin Struct Biol* **14**, 208-216
21. Tordai, H., Nagy, A., Farkas, K., Banyai, L., and Patthy, L. (2005) Modules, multidomain proteins and organismic complexity. *FEBS J* **272**, 5064-5078
22. Bigotti, M. G., and Clarke, A. R. (2005) Cooperativity in the thermosome. *J Mol Biol* **348**, 13-26
23. Kafri, G., and Horovitz, A. (2003) Transient kinetic analysis of ATP-induced allosteric transitions in the eukaryotic chaperonin containing TCP-1. *J Mol Biol* **326**, 981-987
24. Korobko, I., Nadler-Holly, M., and Horovitz, A. (2016) Transient Kinetic Analysis of ATP Hydrolysis by the CCT/TRiC Chaperonin. *J Mol Biol* **428**, 4520-4527
25. Bigotti, M. G., Bellamy, S. R., and Clarke, A. R. (2006) The asymmetric ATPase cycle of the thermosome: elucidation of the binding, hydrolysis and product-release steps. *J Mol Biol* **362**, 835-843
26. Nitsch, M., Walz, J., Typke, D., Klumpp, M., Essen, L. O., and Baumeister, W. (1998) Group II chaperonin in an open conformation examined by electron tomography. *Nat Struct Biol* **5**, 855-857
27. Gutsche, I., Mihalache, O., and Baumeister, W. (2000) ATPase cycle of an archaeal chaperonin. *J Mol Biol* **300**, 187-196
28. Schoehn, G., Hayes, M., Cliff, M., Clarke, A. R., and Saibil, H. R. (2000) Domain rotations between open, closed and bullet-shaped forms of the thermosome, an archaeal chaperonin. *J Mol Biol* **301**, 323-332
29. Paul, D. M., Beuron, F., Sessions, R. B., Brancaccio, A., and Bigotti, M. G. (2016) Internal (His)(6)-tagging delivers a fully functional hetero-oligomeric class II chaperonin in high yield. *Sci Rep* **6**, 20696
30. Edgar, R. C. (2004) MUSCLE: multiple sequence alignment with high accuracy and high throughput. *Nucleic Acids Res* **32**, 1792-1797
31. Pettersen, E. F., Goddard, T. D., Huang, C. C., Couch, G. S., Greenblatt, D. M., Meng, E. C., and Ferrin, T. E. (2004) UCSF Chimera--a visualization system for exploratory research and analysis. *J Comput Chem* **25**, 1605-1612
32. Krivov, G. G., Shapovalov, M. V., and Dunbrack, R. L., Jr. (2009) Improved prediction of protein side-chain conformations with SCWRL4. *Proteins* **77**, 778-795
33. McIntosh-Smith, S., Price, J., Sessions, R. B., and Ibarra, A. A. (2015) High performance in silico virtual drug screening on many-core processors. *The international journal of high performance computing applications* **29**, 119-134

34. Harder, K. W., Owen, P., Wong, L. K., Aebersold, R., Clark-Lewis, I., and Jirik, F. R. (1994) Characterization and kinetic analysis of the intracellular domain of human protein tyrosine phosphatase beta (HPTP beta) using synthetic phosphopeptides. *Biochem J* **298 (Pt 2)**, 395-401
35. Weiss, C., and Goloubinoff, P. (1995) A mutant at position 87 of the GroEL chaperonin is affected in protein binding and ATP hydrolysis. *J Biol Chem* **270**, 13956-13960
36. Wood, C. W., Bruning, M., Ibarra, A. A., Bartlett, G. J., Thomson, A. R., Sessions, R. B., Brady, R. L., and Woolfson, D. N. (2014) CCBuilder: an interactive web-based tool for building, designing and assessing coiled-coil protein assemblies. *Bioinformatics* **30**, 3029-3035
37. Wood, C. W., Heal, J. W., Thomson, A. R., Bartlett, G. J., Ibarra, A. A., Leo Brady, R., Sessions, R. B., and Woolfson, D. N. (2017) ISAMBARD: an open-source computational environment for biomolecular analysis, modelling and design. *Bioinformatics*
38. Monera, O.D., Kay, C.M., and Hodges, R.S. (1994) Protein denaturation with guanidine hydrochloride or urea provides a different estimate of stability depending on the contributions of electrostatic interactions. *Protein Sci* **3**, 1984-1991
39. Staniforth, R.A., Bigotti, M.G., Cutruzzola, F., Allocatelli, C.T., and Brunori, M. (1998) Unfolding of apomyoglobin from Aplysia limacina: the effect of salt and pH on the cooperativity of folding. *J Mol Biol* **275,** 133-148
40. Chaston, J. J., Smits, C., Aragao, D., Wong, A. S., Ahsan, B., Sandin, S., Molugu, S. K., Molugu, S. K., Bernal, R. A., Stock, D., and Stewart, A. G. (2016) Structural and Functional Insights into the Evolution and Stress Adaptation of Type II Chaperonins. *Structure* **24**, 364-374
41. Kapatai, G., Large, A., Benesch, J. L., Robinson, C. V., Carrascosa, J. L., Valpuesta, J. M., Gowrinathan, P., and Lund, P. A. (2006) All three chaperonin genes in the archaeon Haloferax volcanii are individually dispensable. *Mol Microbiol* **61**, 1583-1597
42. Jiang, Y., Douglas, N. R., Conley, N. R., Miller, E. J., Frydman, J., and Moerner, W. E. (2011) Sensing cooperativity in ATP hydrolysis for single multisubunit enzymes in solution. *Proc Natl Acad Sci U S A* **108**, 16962-16967
43. Douglas, N. R., Reissmann, S., Zhang, J., Chen, B., Jakana, J., Kumar, R., Chiu, W., and Frydman, J. (2011) Dual action of ATP hydrolysis couples lid closure to substrate release into the group II chaperonin chamber. *Cell* **144**, 240-252

44. Zhang, J., Baker, M. L., Schroder, G. F., Douglas, N. R., Reissmann, S., Jakana, J., Dougherty, M., Fu, C. J., Levitt, M., Ludtke, S. J., Frydman, J., and Chiu, W. (2010) Mechanism of folding chamber closure in a group II chaperonin. *Nature* **463**, 379-383
45. Pereira, J. H., Ralston, C. Y., Douglas, N. R., Meyer, D., Knee, K. M., Goulet, D. R., King, J. A., Frydman, J., and Adams, P. D. (2010) Crystal structures of a group II chaperonin reveal the open and closed states associated with the protein folding cycle. *J Biol Chem* **285**, 27958-27966
46. Lopez, T., Dalton, K., Tomlinson, A., Pande, V., and Frydman, J. (2017) An information theoretic framework reveals a tunable allosteric network in group II chaperonins. *Nat Struct Mol Biol*
47. Clare, D. K., Stagg, S., Quispe, J., Farr, G. W., Horwich, A. L., and Saibil, H. R. (2008) Multiple states of a nucleotide-bound group 2 chaperonin. *Structure* **16**, 528-534

FIGURE LEGENDS

Figure 1. *Ta* thermosome mutants in the ATP-binding pocket of the α and β subunits. A) Left, side view of the ATP·AlF3 bound *Ta* thermosome (from PDB: 1A6D) with a couple of adjacent α and β subunits in light blue and magenta, respectively. The His_6-tags protruding from each α subunit are in space-filling representation. The ATP-binding pocket of the α subunit is boxed and enlarged in the right panel, where the residues involved in ATP-binding (Thr97 and Thr157) and hydrolysis (Asp94) are also indicated. B) Superposition of the wild-type ATP-binding pocket (blue) with that mutated at residue Asp93β/94α to either Lys or Ala (purple), that mutated at Thr96β/97α to Val (green) and that mutated at Thr157α/158β to Ala (light grey). C) Multiple alignment of the two *T. acidophilum* subunits sequences with a selection of orthologous sequences; only the region of the ATP-binding pocket is shown. The mutated residues located within the region of the conserved P-loop (highlighted in blue) are indicated by the red and the green arrow (Asp 94α/93β and Thr 97α/96β, respectively), those outside the P-loop, Thr157α/158β, are indicated by the light blue arrow. Sequence codes: Ta: *Thermoplasma acidophilum*; Ec: *Escherichia coli*; Mm: *Methanococcus maripaludis*; Ss: *Sulfolobus solfataricus*; Ss: *Saccharomyces cerevisiae* str. S288c.

Figure 2. **Different oligomeric states of the *Ta* thermosome mutants.** A) SDS-PAGE of the purified mutants, identified on top of each lane. Masses of significant bands from the molecular weight marker (Rainbow Broad Range MWM, Thermo Fisher Scientific) are reported on the left, the α and β bands are indicated on the right. B) Native-PAGE of a representative set of purified mutants, all running as ≅1MDa complexes. MWM: Molecular weight marker (Native Mark, Life Technologies). C) Size exclusion chromatography profile of the purified mutant D93Kβ as run on a high resolution Superose 6 gel filtration column. The elution profiles of all the other mutants are similar, with a main peak with a retention time corresponding to a molecular weight of ≅950kDa (indicated by the arrow). The minor peaks eluting at longer retention times correspond to small α/β oligomers (mainly dimers) and single subunits; when a homogeneous population of hexadecamers was needed, it was isolated as the main peak eluting from a similar, semi-preparative size-exclusion chromatography.

Figure 3. Calculation of interface energies by MD simulation and BUDE. A) Illustrates the calculation of the interaction energy of subunit interfaces using BUDE. B) Schematic example of the interfaces considered in the energy calculations for one subunit. Hence, the global energy for the subunit in position 2 was calculated comprising contacts made with all its neighbours 2→1, 3, 4, 5 & 6. Separate energies based on the single

contributions from 1→2, 2→3 and 2→5 were also calculated and subtracted from the global energy, indicating the relative importance of the diagonal interactions 2→4 and 2→6. C) The calculated timepoint energies have been averaged for each subunit and presented graphically for the whole $\alpha_8\beta_8$, α_{16} and β assemblies. D) BUDE calculated global energies from structures at 3 ns intervals. The complete set of energies calculated, including those of the mutants, are reported in Table 2.

Figure 4. ATP-ase and refolding activities of the WT thermosome and its mutants. A) ATPase activity of the WT $\alpha_8\beta_8$ thermosome (open circles) and of the hydrolysis mutants D93Kβ $\alpha_8\beta_8$ (closed squares) and D94Aα $\alpha_8\beta_8$ (open squares) at 55°C as a function of ATP concentration. B) ATPase activity of the α-only thermosome (α_{16}) at 55°C as a function of ATP concentration. Inset: linear dependence of the maximum hydrolytic rate of the two hydrolysis mutants on thermosome concentration. C) Substrate refolding activity at 55°C, in the absence (empty symbols) and presence (filled symbols) of ATP, of the wt thermosome (red triangles) and of the hydrolysis mutants D93Kβ $\alpha_8\beta_8$ (green squares) and D94Aα $\alpha_8\beta_8$ (blue diamonds). The activity of the native substrate (T*a* RhaD) is indicated by the black closed circles, and the recovery in activity of unfolded T*a* RhaD upon refolding in the absence of thermosome is illustrated by the black open circles. Results of such experiments in the presence of the homo-oligomeric complexes WT α_{16} and D94Kα α_{16} are reported in the inset. D) Substrate refolding activity at 55°C in the absence (empty symbols) and presence (filled symbols) of ATP, of the WT $\alpha_8\beta_8$ thermosome (red triangles) and of the binding mutants T158Aβ $\alpha_8\beta_8$ (green squares) and T157Aα $\alpha_8\beta_8$ (blue diamonds). The refolding yields of the WT $\alpha_8\beta_8$ thermosome and all mutants are reported in Table 1. Each data point reported is the average of at least five independent experiments.

Figure 5. Schematics of proposed ATPase cycle of the ATP-binding (panel A) and hydrolysis (panel B) mutants and of the WT thermosome (panel C). The circles indicate the apo-state, the squares the ATP-bound state and the hexagons the post-hydrolysis closed state; the asterisk marks mutated subunits. For graphical clarity, only one of the 4 pairs of adjacent α-β subunits per ring is displayed. A) Proposed rearrangements of the ATP-binding mutants. The scheme shows how the ATPase cycle in the unmodified subunit can be blocked either at the ATP hydrolysis step (population of complex 1) or at the product release step (population of complex 2, boxed). B) Proposed rearrangements of the ATP-hydrolysis mutants upon ATP binding. The β (tight) subunit has a higher ATP-ase activity than the α (weak), but both need to bind ATP to allow cycling of the adjacent subunit. For graphical simplicity, the scheme only presents the case in which ATP binds the β subunit first, although also the opposite is in principle possible. C) Proposed ATP-ase cycle for the wild-type *Ta* thermosome based on the asymmetric behaviour and allostery displayed by the two subunits. The events are

coordinated by the allosteric requirement for ATP to be bound to one subunit for the next one to release the hydrolysis products and be re-engaged in the cycle. Only the case in which ATP binding to one subunit is indispensable for the release of substrates (ADP and phosphate) from the neighboring one is reported (see Discussion for details).

Figure 1

Figure 1

A

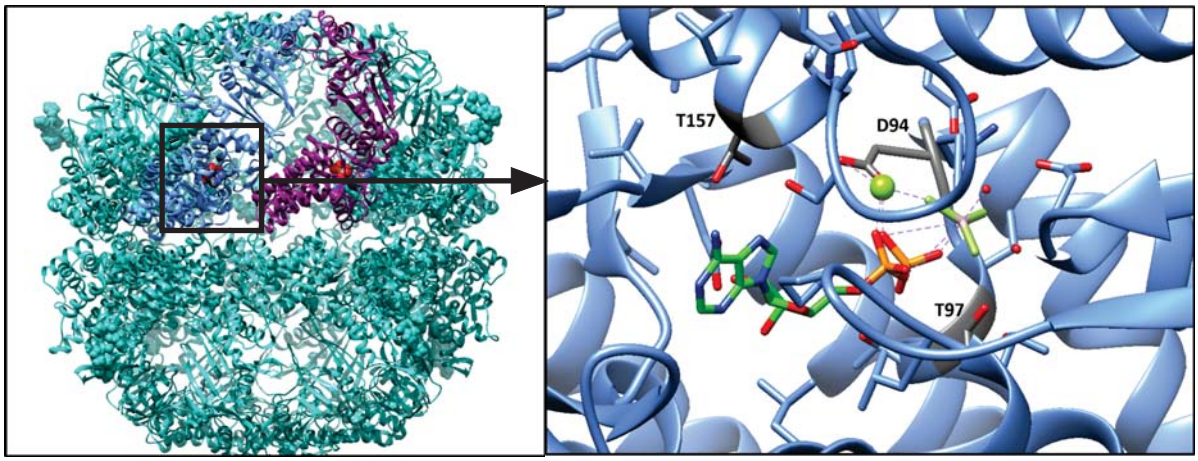

B

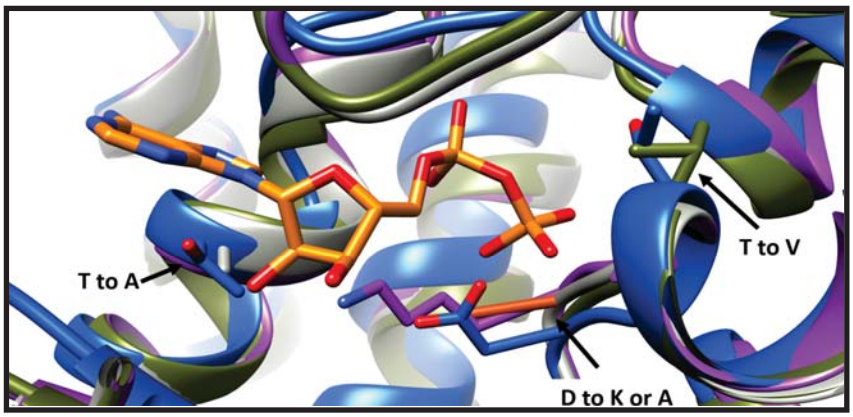

C

```
Ec_GroEL      73 MVKEVASKTSDNAGDGTTTATVLAQAFIREGMK-AVAA-G//..143 --EIAQVGAISANSD
Sc_theta      84 VLVMATEQQKIDMGDGTNLVMILAGELLNVSEK-LISM-G//..156 KNELLKMIKPVISSK
Sc_eta        82 TLVDISFAQDAEVGDGTTSVTILAGELMKEAKP-FLEE-G//..155 RELLEQGARTAMSSK
Sc_zeta       75 LIARAAAAQDEITGDGTTTVVCLVGELLRQAHR-FIQE-G//..147 REFLLQVARSSLLTK
Sc_epsilon   103 LLVQLSKSQDDEIGDGTTGVVVLASALLDQALE-LIQK-G//..177 RDFLLFAAKTSLGSK
Sc_delta      77 MLVEVSAAQDSEAGDGTTSVVILTGALLGAAER-LLNK-G//..147 REQLVEAASTSLSSK
Sc_gamma      77 SMLELSFTQDEEVGDGTTTVIILAGETLAQCAPYLIEK-N//..148 DAAMKKIIQASIGTK
Sc_beta       76 VLVNISKVQDDEVGDGTTSVTVLSAELLREAEK-LIDQSK//..150 REDLIHIAKTTLSSK
Sc_alpha      82 ILVELAQQQDREIGDGTTSVVIIASELLKRANE-LVKN-K//..153 KETLINIAKTSMSSK
Ss_gamma      77 LLIETAKTVDTEVGDGTTSVVVLAGLLLEKAED-LLNQ-K//..147 RKIVHDIVYTTLSSK
Ss_beta       90 LLVQIAKCQDEETADGTKTAVTLAGELAKKAED-LLYK-E//..160 TDVLRKVALTSLGSK
Ss_alpha      77 LLVEAAKAQDAEVGDGTTSAVVLAGALLEKAES-LLDQ-N//..153 RDTLRKIAFTTLASK
Mm_alpha      77 MLIEVAKTQEKEVGDGTTTAVVVAGELLRKAEE-LLDQ-N//..147 KEILTKIAMTSITGK
Ta_alpha      80 MIVEVSKAQDTAVGDGTTTAVVLSGELLKQAET-LLDQ-G//..150 --TLRKIALTALSGK
Ta_beta       79 MMVEVSKTQDSFVGDGTTTAVIIAGGLLQQAQG-LINQ-N//..149 KALLLKMAQTSLNSK
```

Figure 2

Figure 2

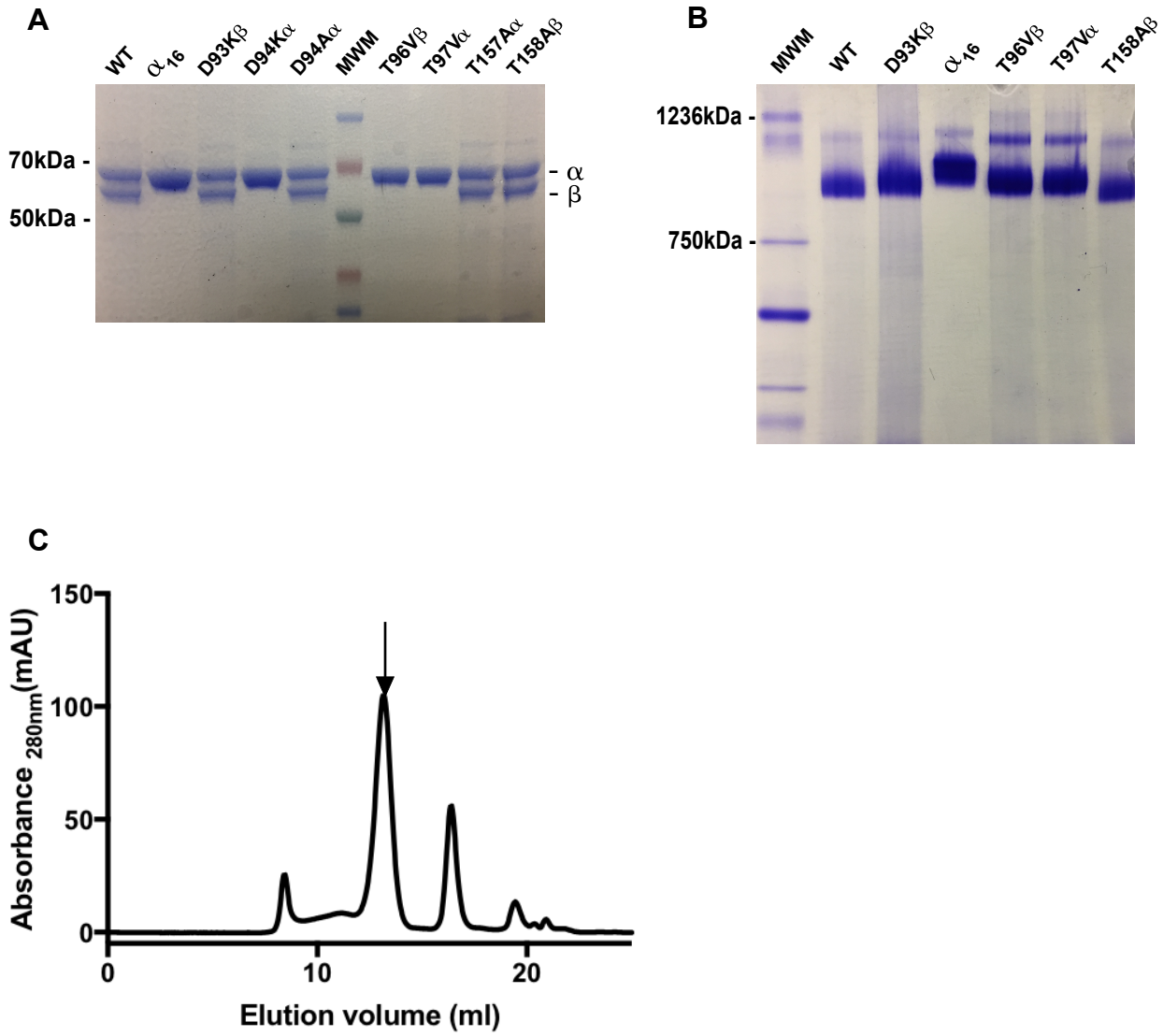

Figure 3

Figure 3

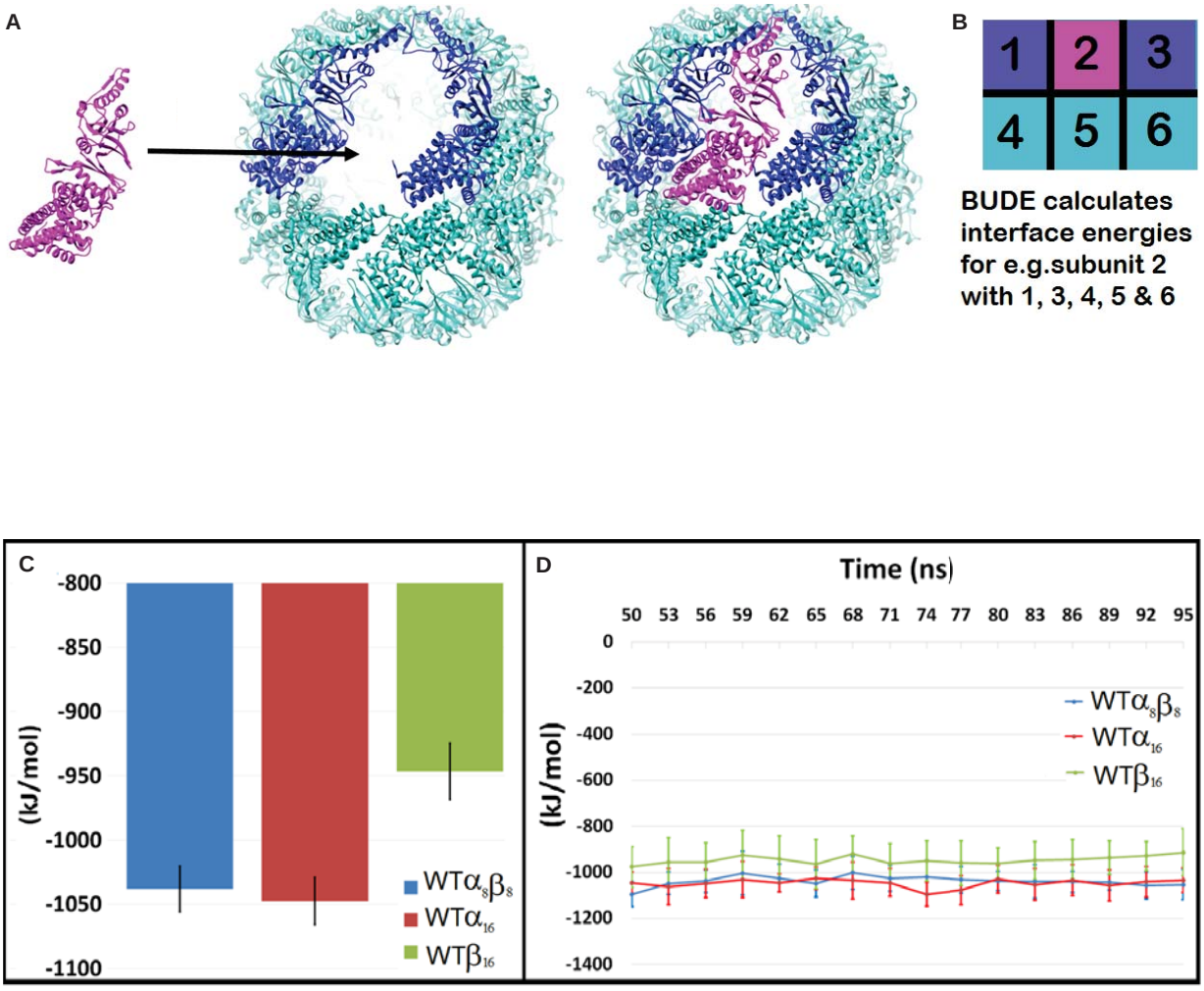

Figure 4

Figure 4

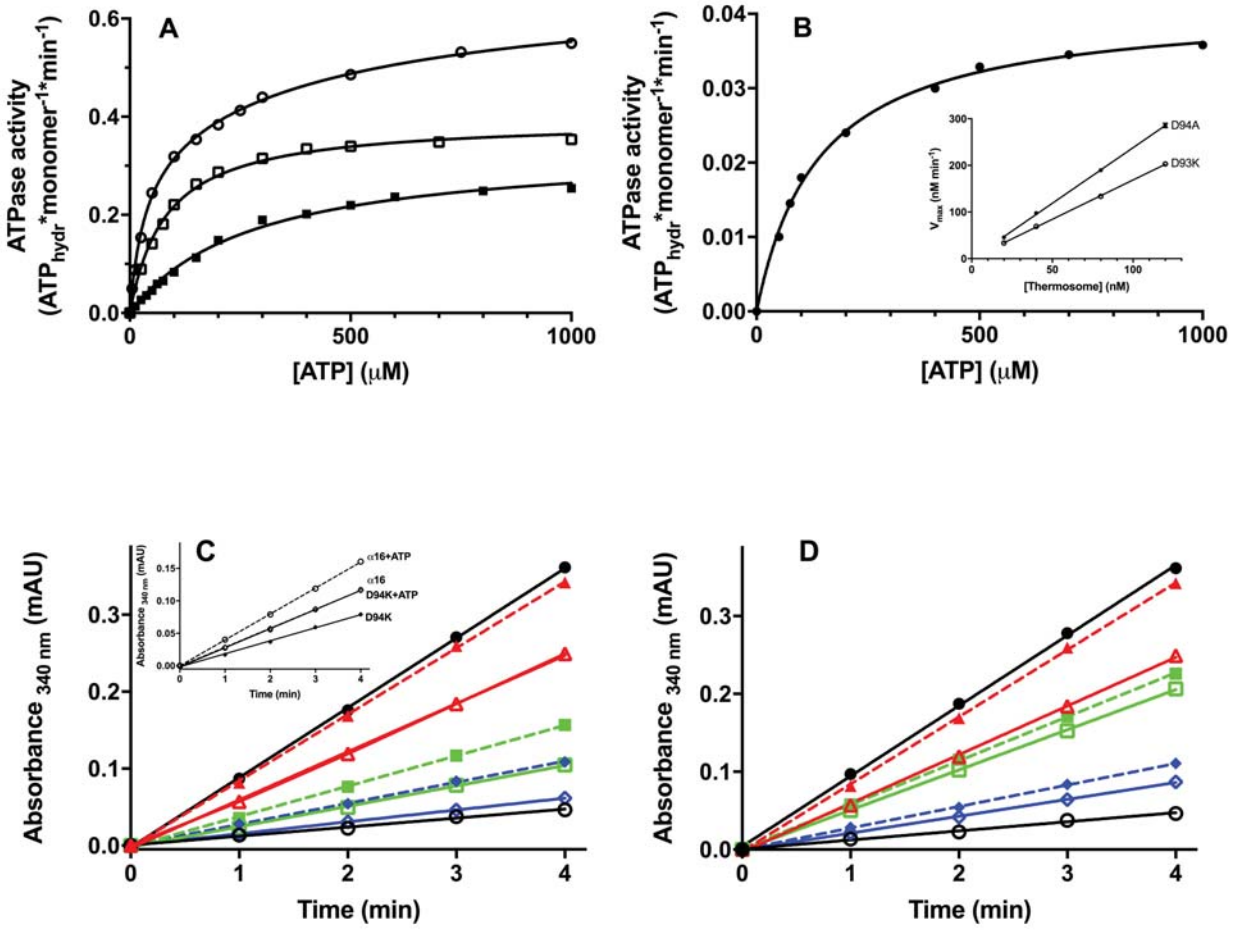

Figure 5

Figure 5

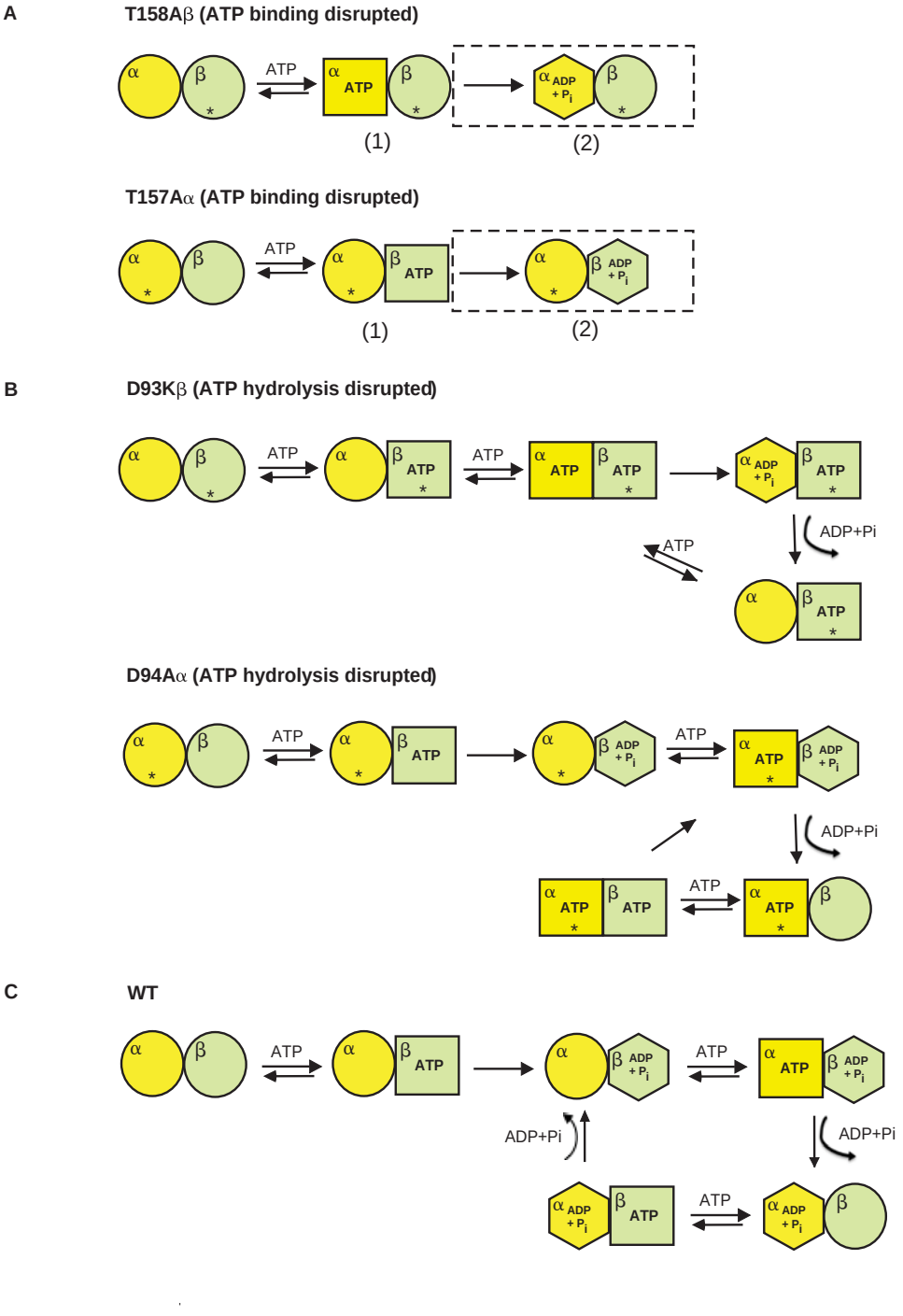

Table 1. Steady state ATPase and refolding activities of the *Ta* thermosome and its variants.

Effect of mutation	*Ta* therm	Complex	ATP-Hydrolysis	Refolding[1] (no ATP) %	Refolding[1] (+ATP) %
	WT	$\alpha_8\beta_8$	K_{M1}= 15 µM ± 1.65 k_{cat1}= 2.15 ± 0.12 K_{M2}= 370 µM ± 46 k_{cat2}= 3.2 ± 0.15	68 ± 3.4	95 ± 2.9
	WTα_{16}	α_{16}	K_M= 140 µM ± 15.7 k_{cat} = 0.33 ± 0.015	33 ± 1.7	44 ± 2
ATP hydrolysis blocked	**D94Kα**	α_{16}	None detected	21 ± 2.9	31 ± 2.6
	D94Aα	$\alpha_8\beta_8$	K_M= 82 µM ± 8.7 k_{cat} = 2.4 ± 0.09	17 ± 2.2	32 ± 2.7
	D93Kβ	$\alpha_8\beta_8$	K_M= 285 µM ± 35 k_{cat} = 1.7 ± 0.14	28.5 ± 2.6	43 ± 2.8
ATP binding blocked	**T97Vα**	α_{16}	None detected	No effect	No effect
	T96Vβ	α_{16}	See WTα_{16}	See WTα_{16}	See WTα_{16}
	T157Aα	$\alpha_8\beta_8$	None detected	24 ± 2.5	30.5 ± 2.1
	T158Aβ	$\alpha_8\beta_8$	None detected	57 ± 2.2	62.6 ± 1.9

The k_{cat} values are expressed in moles ATP_{hydr}/(mol active sites)*min

[1]: expressed as recovery in activity relative to the activity of the native substrate.

The spontaneous (i.e. in the absence of thermosome) refolding yield of unfolded RhaD is 13±2 %.

Table 2. BUDE calculated interface energies for the respective assemblies

α–β	Intra-ring	sd	Inter-ring	sd	Inter α	sd	Inter β	sd	nrg from subs	nrg from seps	difference
WT	-450	12	-114	11	-114	12	-114	9	-1038	-1013	-25
D94Aα	-444	15	-117	9	-118	8	-115	10	-1025	-1005	-20
D93Kβ	-443	13	-106	10	-111	8	-102	10	-1015	-992	-23
T157Aα	-435	16	-115	11	-118	9	-111	11	-1009	-986	-23
T158Aβ	-443	15	-111	10	-116	7	-105	10	-1022	-997	-24
T97Vα	-438	14	-123	9	-104	10	-113	13	-1014	-999	-15
T96Vβ	-442	12	-130	8	-106	11	-118	16	-1031	-1015	-16
D94Kα	-440	15	-116	10	-122	7	-110	8	-1025	-997	-28
α–α											
WTα_{16}	-447	13	-137	8	-137	8	N/A	N/A	-1047	-1030	-17
D94Aα	-453	14	-144	6	-144	6	N/A	N/A	-1048	-1050	2
D94Kα	-445	13	-141	10	-141	10	N/A	N/A	-1065	-1031	-34
T157Aα	-449	12	-145	8	-145	8	N/A	N/A	-1063	-1043	-20
T97Aα	-446	14	-146	5	-146	5	N/A	N/A	-1055	-1037	-18
β–β											
WT	-401	13	-123	5	N/A	N/A	-123	5	-946	-925	-21

forms αβ
only forms αα
does not form

The background color (see color key) denotes whether the assembly is achieved *in vitro*. All energies are expressed in kJ mol^{-1}. sd: standard deviation (in kJ mol^{-1}). **nrg from subs:** energies from subunits, refers to the *BUDE* energy calculated when each subunit is docked back into the whole assembly over time-points of 20ns simulations and then averaged over time and subunit energies. This gives an indication of strength of interaction between all the subunit interfaces, both inter and intra ring. **nrg from seps** – refers to the BUDE energies calculated per subunit interface, separating the intra-ring (side-by-side) interaction energies from the inter-ring energies designated by stacked subunits (α-α and β-β). **difference** – difference between the first and second method. It indicates the relative importance of the diagonal interaction in the inter-ring interface.

Figure S1

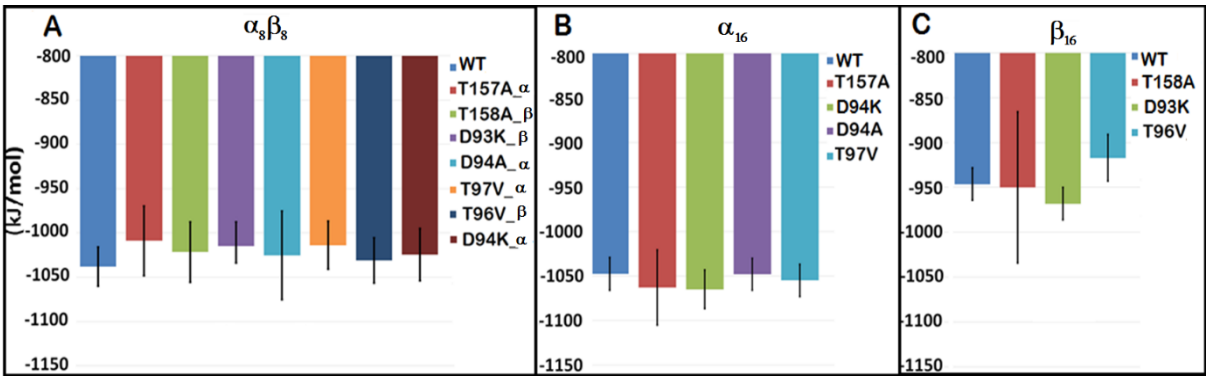

Figure S1. Interface energies for the ATP binding and hydrolysis mutants. Global BUDE subunit interface energies are shown averaged over all subunits and 50 ns trajectories to determine whether mutations made to disrupt ATP binding and hydrolysis affected interface energies, when compared with their wild-type equivalents. (A) BUDE-calculated global subunit interface energies for the mutations made in the $\alpha_8\beta_8$ complexes. (B) BUDE-calculated global subunit interface energies for the mutations made in α_{16} assemblies. (C) BUDE-calculated global subunit interface energies for the mutations for beta$_{16}$ assemblies.

Figure S2

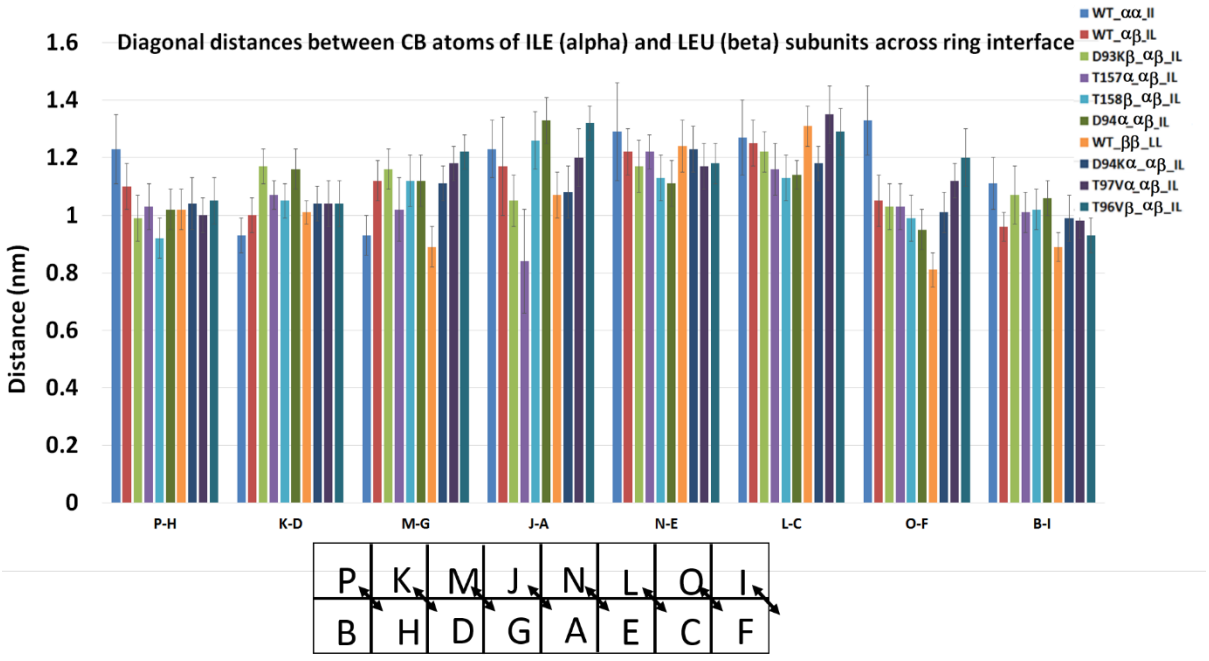

Figure S2. Diagonal distances between subunits for the WT and mutant assemblies averaged over time. The diagonal distances between residues that come into close contact diagonally across the ring-to-ring interface as indicated by the arrows in box, with chain labels where A,B,C,D,M,N,O&P are α subunits and E,F,G,H,I,J,K & L are β subunits in the $\alpha_8\beta_8$ assemblies. IL denotes the average distances between the C-beta carbon of isoleucine sidechain in an α subunit and the C-beta of a leucine sidechain in a β subunit.